Journal of Science and Technology – Smart Systems and Devices
Volume 36, Issue 1, January 2026, 060-070

Design and Optimization of High-Efficiency Ceiling Fan Blades

Bao Duy Thanh Tran[1], Duc Huy Ta[2], Dinh Quan Tran[2], Dinh Quy Vu[1] , Thi Tuyet Nhung Le[1*]
[1]Hanoi University of Science and Technology, Ha Noi, Vietnam
[2] Gcool Joint Stock Company, Ha Noi, Vietnam
[*]Corresponding author email: nhung.lethituyet@hust.edu.vn

Abstract

The study presents the design and optimization process for high-performance ceiling fans aimed at energy savings and environmental protection. Utilizing Computational Fluid Dynamics (CFD) numerical simulations with the k-ω SST turbulence model and the multi-reference frame (MRF) method, various fan blade configurations were evaluated to enhance airflow and improve energy consumption efficiency. The design process focused on selecting the aerodynamic profile (airfoil), optimizing the twist angle, and distributing the chord length. Among the tested options, the optimized version yielded superior results in airflow distribution, torque, and noise characteristics. The grid convergence analysis with 11.5 million elements validated the accuracy of the simulations. The addition of winglets helped reduce tip vortex phenomena and sound intensity, lowering it by up to 20 dB. A frequency spectrum analysis model using the Fast Fourier Transform (FFT) was applied to assess the sound characteristics in detail and identify noise-causing frequency components. The final design meets technical requirements and manufacturability, achieving optimal performance at a speed range of 220–225 rpm for the 5-blade configuration and 265 rpm for the 3-blade configuration. Energy performance parameters were measured according to Vietnam national standards (TCVN) for electric fans, validating the simulation results and ensuring suitability under real operating conditions.

Keywords: Aerodynamic, ceiling fan, design and optimization, fan blades.

1. Introduction

Ceiling fans are a common and essential component in air conditioning and cooling systems, particularly in countries with tropical climates. Owing to their low energy consumption and high cooling efficiency, ceiling fans have become an effective solution for improving thermal comfort in enclosed spaces. However, the operational performance of ceiling fans depends on various factors, including the motor, blade design, number of blades, rotational speed, and airflow distribution model.

Previous studies have analyzed the fluid dynamics of ceiling fans in empty room conditions, as well as the impact of design factors on fan performance. Ankuar *et al.* (2004) experimentally analyzed the airflow field of ceiling fans, identifying eight distinct regions in the airflow circulation model [1]. Studies have also shown that blade structure significantly affects velocity distribution and overall performance. Parker *et al.* (2000) demonstrated that using aerodynamically shaped blades can increase airflow by up to 21% while significantly reducing energy consumption [2]. Additionally, Falahat (2011) developed a predictive model for airflow velocity and validated the results through numerical simulations [3]. Research by Son *et al.* (2009) also emphasized that thermal comfort in a room is strongly influenced by the vertical wind speed of the fan [4].

In recent years, aeroacoustic noise generated by rotating blades such as ceiling fans, axial fans, and propellers has emerged as a significant challenge in both product development and environmental comfort. In addition to energy efficiency and aerodynamic performance, noise reduction has become a vital design objective, especially for indoor environments where acoustic comfort is essential.

To address this challenge, advanced numerical models such as Detached Eddy Simulation (DES) have been widely adopted to simulate unsteady flow structures and their associated sound generation mechanisms. DES offers a hybrid approach that captures large turbulent eddies in the flow field (like Large Eddy Simulation - LES), while retaining computational efficiency near walls (like Reynolds-Averaged Navier-Stokes - RANS). This makes DES particularly suitable for predicting aeroacoustic behavior in fan applications.

Pioneering studies such as Kusano *et al.* (2010) [5] applied DES to predict aerodynamic sound from open rotor fans, while Kusano *et al.* (2025) [6] used adjoint-based optimization with a DES framework to minimize

p-ISSN 3093-3285
e-ISSN 3093-3315
https://doi.org/10.51316/jst.187.ssad.2026.36.1.8
Received: Jun 4, 2025; Revised: Sep 3, 2025;
Accepted: Sep 15, 2025; Online: Dec 20, 2025.

cavity-induced noise at low Mach numbers. These studies demonstrated the ability of DES to resolve fine-scale vortices that contribute to tonal and broadband noise.

Beyond simulation techniques, blade geometry has been shown to play a key role in noise reduction. For instance, Vaezi *et al.* (2024) [7] examined the influence of winglet cant angles affect both aerodynamic and acoustic performance, revealing significant sound pressure level (SPL) reductions with geometric tuning. Similarly, Xu *et al.* (2024) [8] investigated the aeroacoustics interactions of coaxial rotors, highlighting the impact of self-interference effects on sound pressure levels.

Haolin *et al.* (2025) [9] introduced a multi-objective adjoint optimization strategy that simultaneously balances aerodynamic and aeroacoustics targets, reflecting the growing trend of integrated noise-aware design. Building on that, Greschner *et al.* (2008) [10] applied DES to simulate sound radiation from a Rod-Airfoil configuration using the Lighthill Ffowcs Williams-Hawkings (FW-H) analogy, providing direct access to pressure-based sound sources in the simulation domain. Supporting this evolution, foundational works such as Hirschberg and Rienstra (2004) [11] provided essential theory in aeroacoustics, while Maizi *et al.* (2017) [12] demonstrated practical noise reduction strategies through blade shape modifications in horizontal wind turbines. Both studies confirm that blade-tip vortices and trailing-edge flows are key contributors to low-frequency noise.

For a comprehensive understanding of DES modeling and implementation, Mockett (2009) [13] provides an in-depth review, while Michel *et al.* (2010) [14] demonstrate the effectiveness of DES and hybrid methods in aerospace rotorcraft applications, highlighting their versatility for complex geometries and turbulent flows.

Building on these findings, the present study proposes a comprehensive design and optimization framework for high-performance ceiling fan blades. Using airfoil-based profiles, customized chord and twist distributions, and numerical simulations with DES coupled with Fast Fourier Transform-based (FFT-based) spectral analysis, the aerodynamic and aeroacoustic characteristics are evaluated in detail. The study also explores tip-rounding strategies, demonstrating a noise reduction of up to 20dB compared to unrounded tips-an outcome consistent with modern aeroacoustic suppression techniques applied in aircraft wing design.

2. Airfoil Comparison

An airfoil is a streamlined aerodynamic shape that serves as the primary cross-section of an aircraft wing and a propeller blade. In this context, propellers typically utilize an asymmetric airfoil, such as the NACA 6512 [15, 7]. The airfoil is characterized by a rounded leading edge and a sharp trailing edge, with the distance between them referred to as the chord (c). The upper surface of the airfoil is convex, with the maximum camber reaching 13.3% of the chord length, located approximately 36% from the leading edge, while the lower surface is concave (or sometimes flat) with a maximum camber of 2.4% of the chord length, situated about 64% from the leading edge. This camber is measured from the airfoil's mean line, a reference straight line rather than the thickness of the airfoil. The angle of attack (α) is the angle formed between the mean line and the relative wind velocity.

When the airfoil moves through the air, it generates a pressure differential, with positive pressure forming on the lower surface and negative pressure (suction) on the upper surface. Notably, the suction on the upper surface is often twice as large as the positive pressure on the lower surface, and both types of pressure act in the same direction, to produce a resultant force (F). This force can be analyzed into two components: lift (L), which is perpendicular to the relative wind velocity and is the useful component (providing lift for the aircraft or static pressure for the propeller), and drag (D), which is parallel to the relative wind velocity and represents unwanted resistance to motion. The goal in airfoil design is to achieve a high lift while maintaining a favorable lift-to-drag ratio (L/D). It should be noted that lift, drag, and the L/D ratio vary significantly with the angle of attack.

The lift coefficient of the airfoil is zero at an angle of attack of approximately -8° (for a symmetric airfoil, it is 0°). As the angle of attack increases, the lift coefficient also rises until it reaches a maximum value of about 1.7 at an angle of attack of approximately 15°. This is considered the upper limit of the effective operating range. The L/D ratio reaches its maximum value of 62.4 at an angle of attack of 1°, indicating that the best operating range lies between 1° and about 10°, where the L/D ratio remains high, and airflow is stable. When the angle of attack exceeds 15°, the airfoil will experience a loss of lift (stall) due to the phenomenon of flow separation from the upper surface.

In some cases, particularly when the airflow contains a lot of dust or to reduce costs, thin metal propeller blades may be used instead of airfoils. Compared to the NACA 6512 airfoil, the thin metal profile (e.g., Göttingen 417a) typically has a lower maximum camber, a lower maximum lift coefficient, and a lower maximum L/D ratio, while the angle of attack at which the maximum lift coefficient occurs is also significantly smaller, resulting in a narrower effective operating range. Despite these aerodynamic performance drawbacks, thin metal blades are still favored in certain fan applications, particularly in propeller fans and axial fans in ducts, due to their simple design, ease of manufacturing, and quality control. Below are the characteristics of the airfoil illustrated from Fig. 1 to Fig. 6 [15].

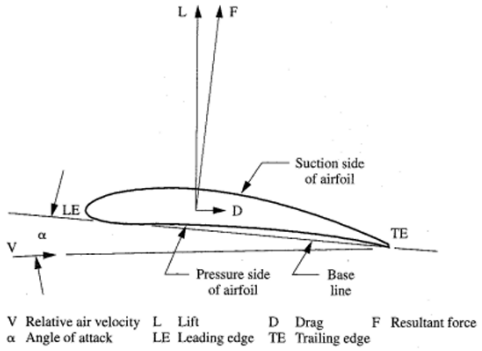

Fig. 1. Airfoil shape (NACA6512)

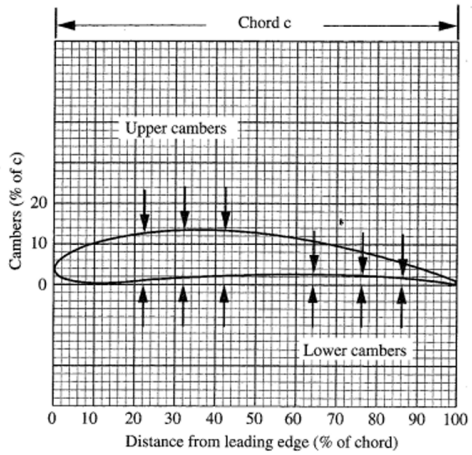

Fig. 2. Parameter of NACA6512

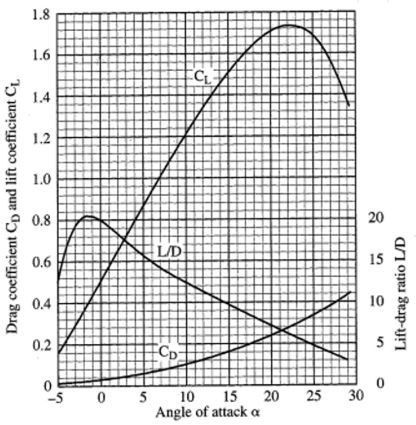

Fig. 3. Graph of lift and drag coefficients versus angle of attack of airfoil

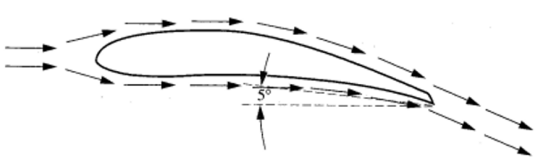

Fig. 4. At 5 degree angle of attack, the flow path following the airfoil at 5 degree

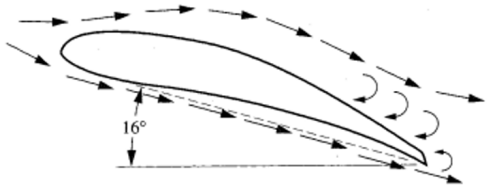

Fig. 5. At 16 degrees, flow separation occuring, causing loss of lift on the airfoil.

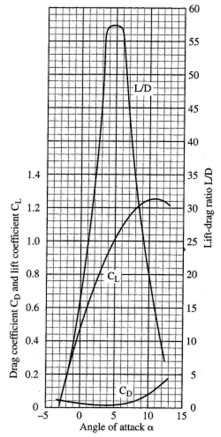

Fig. 6. Aerodynamic characteristics of a flat plate blade

3. Design Process and Numerical Method

3.1. Design Process

The design process for ceiling fans follows several sequential steps (Fig. 7). First, the input parameters for the design problem are defined, including blade diameter, blade load, airflow, and design style. Based on these parameters, a preliminary design model is created using CFTurbo software. Subsequently, the model is subjected to computational fluid dynamics (CFD)

analysis to evaluate flow characteristics, torque, and noise levels. If the simulation results do not meet the requirements, the design will be optimized and the structure refined before re-testing. When the simulation meets the criteria, a physical prototype is produced and undergoes actual measurement processes according to standards at reputable laboratories equipped with the necessary measuring equipment. If the prototype fails to meet the standards, the process will revert to the design optimization step until the design meets the requirements and is ready for commercialization in the market.

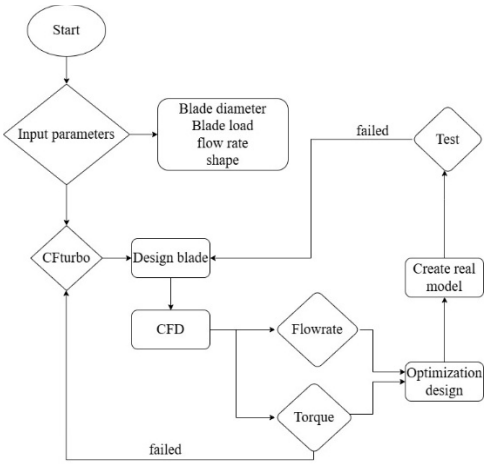

Fig. 7. Design process

Fig. 8. The actual model is built according to the mesurement standard.

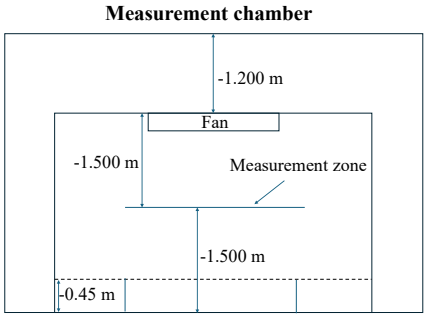

Fig. 9. Description of ceiling fan simulation model

3.2. Simulation Model

To facilitate the comparison, cross-examination, and verification of design results, the simulation model is constructed based on the actual testing model (Fig. 8 and Fig. 9). A measurement chamber with standard dimensions according to the testing method specified in TCVN 7827:2015 for ceiling fans has dimensions of 3×4.5×4.5 m

3.3. Simulation Method

3.3.1. Meshing method

The model is divided into a tetrahedral mesh for optimal contour capturing (Fig. 10 and Fig. 11). The mesh elements are tightly controlled according to the standards of computational mesh quality and are all within the range of good mesh values.

The boundary layer mesh is generated to satisfy the turbulence model used for CFD analysis. On the surfaces of the ceiling fan and the walls of the measurement chamber, 15 layers of boundary layer mesh are initialized with a growth rate of 1.2 to ensure that $y+$ is less than 1, suitable for the turbulence model $k-\omega$ Shear Stress Transport (SST) and advanced turbulence models like DES for time-dependent calculations and aerodynamic noise.

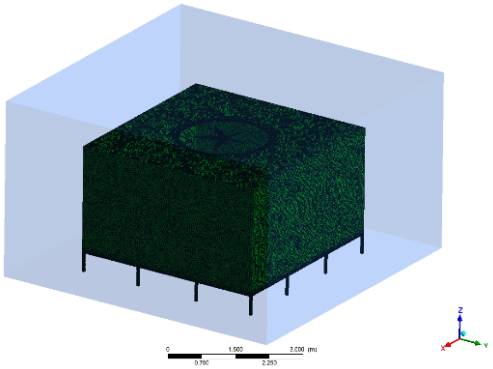

Fig. 10. Measurement Chamber and ceiling fan mesh

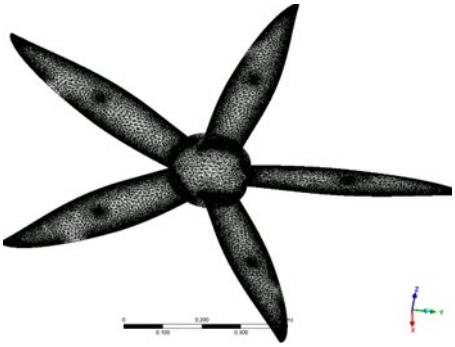

Fig. 11. Blade surface mesh

3.3.2. Numerical method and boundary conditions

To simulate the propeller problem, a method has been developed to optimize the calculation for the rotor machine problem in a steady state, which is the Multiple Reference Frame (MRF) method. The Multiple Reference Frame method is a fluid mechanics simulation technique commonly used to solve problems involving interactions between moving bodies, such as propellers in pumps, cooling fans, or devices with rotating parts in a fluid. MRF is a stable and time-efficient method compared to complex motion simulation methods like Sliding Mesh. This method significantly saves computation time as there is no actual movement of the mesh, reducing computational resources and processing time. Secondly, MRF provides high stability in constant-speed rotational problems, particularly effective when detailed tracking of flow movement is not required. Finally, compared to complex motion methods like Sliding Mesh, MRF is easier to set up and solve in CFD software.

The boundary conditions of the CFD model are presented in Table 1. The *k-ω* SST turbulence model was selected for simulating the ceiling fan in order to achieve results with high accuracy and reliability, adequately capturing the flow phenomena around the ceiling fan and enabling analysis of noise levels during operation. Table 2 describes the abbreviations of the terms used in the model.

Table 1. Boundary condition

Angular velocity [rpm]	**Axist rotation Z(+)/(-)**	**Wall**
205/215/225	-	No slip wall

Table 2. Definitions and terms (SI system)

Symbol	**Defination**
Hub	Blade root (mm)
Shroud	Blade tip (mm)
Chord	Airfoil chord (mm)
RPM	Revolutions per minute
Torque	moment of force (N.m)
P	Power (W)

4. Results and Discussion

In the present work, based on the analysis and simulation results, the governing equations for calculating the fan's flow rate and torque are defined by flow rate and torque equations.

To evaluate the aerodynamic performance of the fan blades, two critical parameters, air flow rate *(Q)* and torque *(τ)*, are calculated.

Flow Rate (Q): This represents the volume of air that moves through the fan's plane per unit of time. It is calculated by integrating the velocity component perpendicular to that plane over the entire area.

$$Q = \int_A \vec{v} \cdot d\vec{A} \quad (1)$$

where:

Q: is the air flow rate (m^3/min).

$\vec{v}$: is the air velocity vector.

$d\vec{A}$: is the differential area vector on the fan's rotational plane.

Torque $(\vec{\tau})$: This represents the rotational resistance that the motor must overcome, calculated by integrating the forces acting on the surface of the fan blades.

$$\vec{\tau} = \vec{r} \times \vec{F} \quad (2)$$

where:

$\vec{\tau}$: is the torque vector (N.m).

$\vec{\tau}$: is the position vector from the center of rotation to a point on the blade surface.

$\vec{F}$: is the force vector (including pressure and viscous shear stress) acting on the surface element dS of the blade (S).

These values were determined through Computational Fluid Dynamics (*CFD*) numerical simulations, employing the *k-ω* SST turbulence model and the Multiple Reference Frame method to ensure high accuracy. The simulation results were then compared and validated against experimental data measured according to the national standard TCVN 7827:2015.

As an example of the design and simulation of ceiling fan blades, the prototype blade "Air" has been developed. Fig. 12 illustrates the ceiling fan blade design created using CFTurbo. This is a modern design inspired by flower petals, representing a combination of functionality and artistry. It ensures both technical performance and industrial aesthetic appeal.

The geometric parameters are presented for investigation with different blade twist angles. Three blade versions as shown in Table 3.

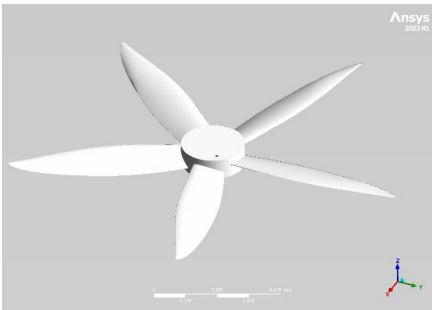

Fig. 12. Geometric model of air ceiling fan

Table 3: Specifications of blade versions

Versions	Twisted hub angle (Deg)	Twisted shroud angle (Deg)	Hub chord length (mm)	Shroud chord length (mm)
Air v1	11	9	107.5	17
Air v2	14	12	107.5	17
Air v3	15	12	107.5	17

4.1. Mesh Convergence Result

To evaluate mesh convergence, the measurement chamber mesh and the stationary region are fixed, while for the rotating region (blade), five mesh models are examined with an increasing number of mesh elements: Mesh 1 (3.2 million elements); Mesh 2 (5.3 million elements); Mesh 3 (8.5 million elements); Mesh 4 (11.5 million elements); Mesh 5 (15.6 million elements). The values of the torque are presented as the observed values for convergence. Through the graph in Fig. 13, it is shown that Mesh 3 is suitable for the simulation model, ensuring convergence capability and computational resource efficiency.

To further assess the reliability and suitability of the computational grid, the distribution chart of the $y+$ values is presented in Fig. 14. The maximum $y+$ value is less than 1, indicating its appropriateness for use with the k-ω SST turbulence model. The majority of $y+$ values are very small at the surface. Therefore, it can once again be concluded that the computational grid is entirely suitable for the computational mesh.

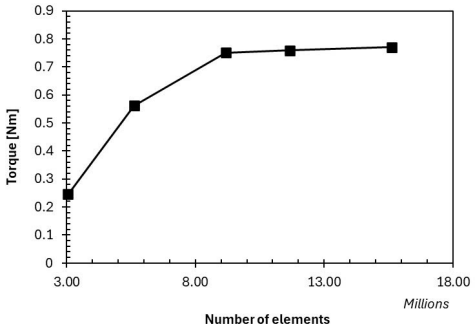

Fig. 13. Grid convergence graph according to torque parameters

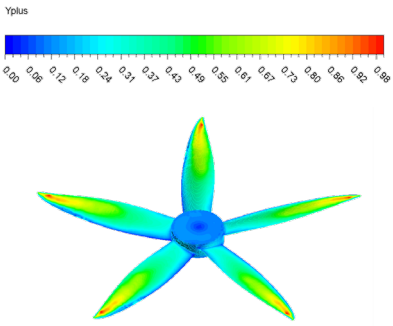

Fig. 14. Distribution of y+ on the blade surface (wall)

4.2. Aerodynamic Characteristics Results

In Fig. 15, we can see that the design and distribution of airflow in version 2 (H14S12) is more aesthetically pleasing and optimized. The airflow angle is approximately 35 degrees from the edge of the blade down to the ground.

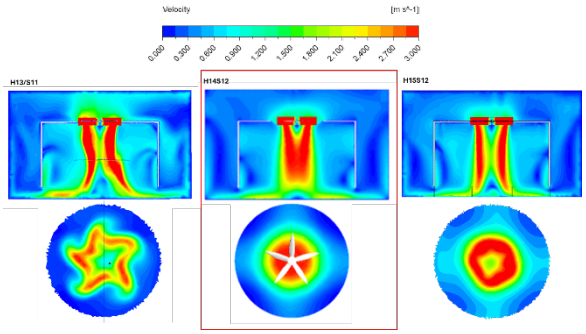

Fig. 15. Velocity field cross-section in the measurement chamber

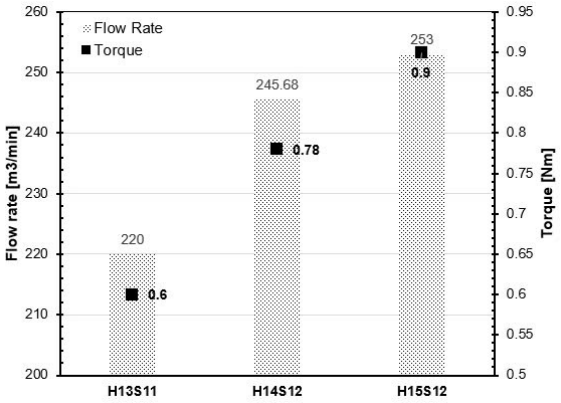

Fig. 16. Flow and torque graphs of three-blade versions

4.3. Energy Efficiency Calculation

The Energy Efficiency Ratio (EER) of a ceiling fan is determined according to the formula:

$$EER = \frac{Q}{P}\ [\mathrm{m}^3/(\mathrm{min}\cdot\mathrm{W})] \tag{3}$$

where:

- Q is the airflow (m^3/min),
- P is the power consumption (W)

According to TCVN 7827:2015, the minimum value EER_{min} depends on the fan diameter D, as shown in Table 4, is classified according to Table 5. From this, the energy efficiency index R is calculated:

$$R = \frac{EER}{EER_{min}} \tag{4}$$

Table 4. Minimum energy efficiency of ceiling fans

Ceiling diameter D (mm)	EER_{min} [$m^3/(min \cdot W)$]
< 900	2.75
$900 \leq D < 1050$	2.79
$1050 \leq D < 1200$	2.93
$1200 \leq D < 1350$	3.04
≥ 1350	3.15

Table 5. Energy efficiency rating

Energy Performance Index *R*	Energy Efficiency Ratio
$1.00 \leq R < 1.15$	1
$1.15 \leq R < 1.30$	2
$1.30 \leq R < 1.45$	3
$1.45 \leq R < 1.60$	4
$R \geq 1.60$	5

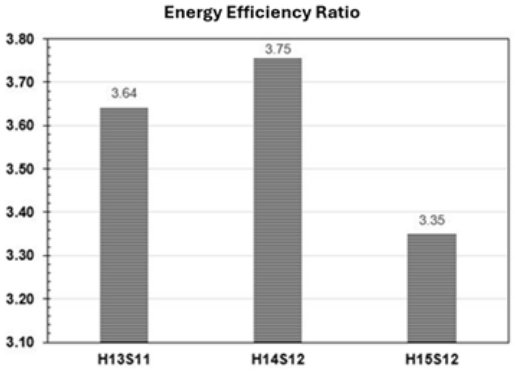

Fig.17. Energy efficiency ratio graph

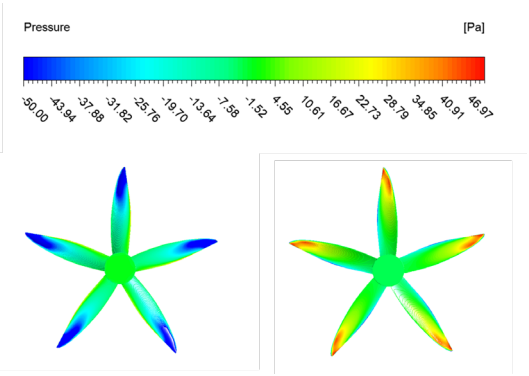

Fig. 18. Pressure distribution on the blades surface (upper and lower surfaces respectively)

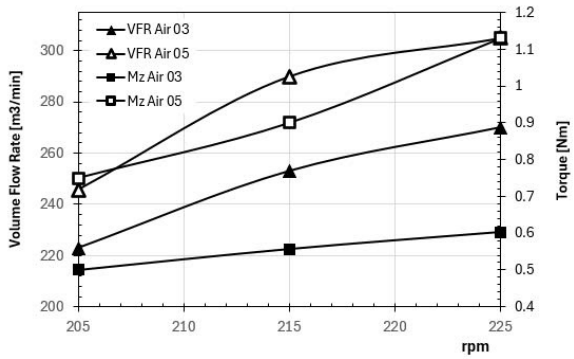

Fig. 19. Flow and torque graphs at different rotational speeds

According to Fig. 15 and Fig. 16, the results indicate that the H14S12 design (Version 2) achieves the optimal performance in terms of energy efficiency (R = 3.75 > 1.6). This result demonstrates that ceiling fans utilizing this blade design can deliver the highest efficiency in the market, exceeding the 5-star rating benchmark by a factor of 2.3. To further evaluate the operational capabilities of the Version 2 blades, a range of speeds was examined for both the 5-blade and 3-blade versions. The results yielded the graphs presented below (Fig. 17 and Fig. 18). For the 5 blades, the effective speed is confirmed to be in the range of 220-225 rpm (Fig. 19).

5. Assessment of the Intensity of Edge Vortex Shedding and Noise

5.1. Aeroacoustic Model

5.1.1. Modeling

In this study, the Aeroacoustic simulation model is implemented using the Detached Eddy Simulation method to accurately predict the noise generation phenomenon from a ceiling fan rotating at a speed of 225 revolutions per minute in an enclosed space. DES is a hybrid model that combines RANS and LES, allowing for detailed simulation of large-scale turbulent flow structures in the far field while maintaining computational efficiency near the wall through RANS. The pressure fluctuations due to the interaction between the blades and the air are recorded at receiver points within the computational domain. The time-dependent pressure data is processed using Fast Fourier Transform (FFT) to obtain the Sound Pressure Level (SPL) spectrum in the frequency domain. The results indicate that the SPL spectrum decreases with increasing frequency, with significant amplitude concentrated in the low-frequency range, reflecting the noise characteristics primarily caused by large-scale turbulence and the near-axis instability effects. The DES model, combined with SPL spectral analysis, enables accurate assessment and quantification of the impact of turbulent flow on the noise generated by the ceiling fan in a closed environment.

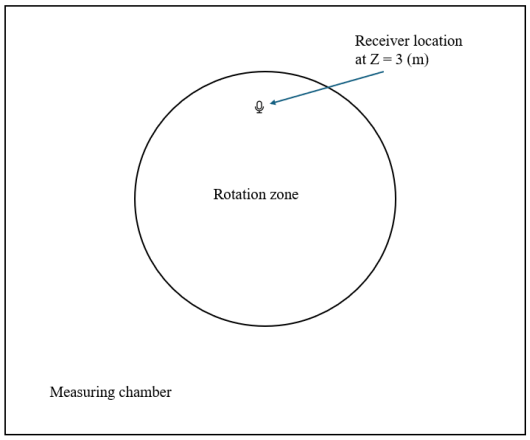

Fig. 20. Receiver location

To obtain the sound map, receivers are positioned at measurement locations, with the receiver at the blade tip being designated as the primary evaluation data, as the blade tip generates vortex tip flows and is the main source of noise from the fan blades (Fig. 20).

5.1.2. Governing equations for aeroacoustic modeling

The aeroacoustic behavior of the ceiling fan blades is modeled by combining aerodynamic flow simulations with sound generation and propagation analysis. The theoretical foundation is based on Lighthill's Acoustic Analogy, enhanced by high-fidelity turbulence modeling using the Detached Eddy Simulation approach, and frequency-domain analysis via the Fast Fourier Transform

Lighthill's Acoustic Analogy

Lighthill (1952) formulated an acoustic analogy that describes the generation of sound by turbulent flows as an inhomogeneous wave equation. The governing equation is written as:

$$\frac{\partial^2 \rho'}{\partial t^2} - c_0^2 \nabla^2 \rho' = \frac{\partial^2 T_{ij}}{\partial x_i \partial x_j} \tag{5}$$

$$\frac{\partial^2 \rho'}{\partial t^2} - c_0^2 \nabla^2 \rho' = \frac{\partial^2 T_{ij}}{\partial x_i \partial x_j} \tag{6}$$

where:

ρ' is the fluctuating (acoustic) density,

c_0 is the speed of sound in the undisturbed medium,

T_{ij} is the Lighthill stress tensor, defined as:

$$T_{ij} = \rho u_i u_j + \left[(p - c_0^2 \rho)\delta_{ij} - \tau_{ij}\right] \tag{7}$$

here:

ρ is the fluid density,

$u_i u_j$ are the velocity components,

p is the pressure,

τ_{ij} is the viscous stress tensor,

δ_{ij} is the Kronecker delta.

This equation models aerodynamic noise as originating from unsteady turbulent sources, especially in regions with strong vortex shedding, such as blade tips.

Detached Eddy Simulation

To accurately capture the turbulent structures that contribute to noise generation, the Detached Eddy Simulation model is employed. DES blends the Reynolds-Averaged Navier–Stokes method near solid boundaries with the Large Eddy Simulation method in free shear flow regions. The turbulence model used in the RANS portion of DES is the Shear Stress Transport (SST) $k-\omega$ model, governed by the following transport equations:

- Turbulent Kinetic Energy (k):

$$\frac{\partial k}{\partial t} + u_j \frac{\partial k}{\partial x_j} = P_k - \beta^* k\omega + \frac{\partial}{\partial x_j}\left[(\nu + \sigma_k \nu_t)\frac{\partial k}{\partial x_j}\right] \tag{8}$$

- Specific Dissipation Rate (ω):

$$\frac{\partial \omega}{\partial t} + u_j \frac{\partial \omega}{\partial x_j} = \alpha \frac{\omega}{k} P_k - \beta\omega^2 + \frac{\partial}{\partial x_j}\left[(\nu + \sigma_\omega \nu_t)\frac{\partial \omega}{\partial x_j}\right] \tag{9}$$

where:

ν is the molecular kinematic viscosity,

ν_t is the eddy viscosity,

P_k is the production term of turbulent kinetic energy,

$\alpha, \beta, \beta^*, \sigma_k, \sigma_\omega$ are model coefficients.

DES automatically switches from RANS to LES based on the local grid resolution and distance from walls, allowing it to resolve large turbulent eddies in the flow field, which are essential contributors to broadband aerodynamic noise.

Sound Pressure Level (SPL) by Fast Fourier Transform (FFT)

The unsteady pressure field obtained from DES is post-processed using the Fast Fourier Transform to convert the time-domain signals at selected acoustic receivers into the frequency domain. The resulting Sound Pressure Level is computed as:

$$SPL(f) = 20 \log_{10}\left(\frac{p_{\text{rms}}(f)}{p_0}\right) \tag{10}$$

where:

$p_{\text{rms}}(f)$ is the root mean square of the pressure fluctuation at frequency f,

p_0 equal 20 μPa is the reference sound pressure in air.

This SPL analysis enables identification of dominant frequencies and quantification of overall acoustic performance, especially in relation to tip vortex noise and shear-layer instabilities.

5.2. Noise Comparison

Result

The maximum recorded noise level is 74.5 dB at the position where the receiver is placed. Due to the blade design featuring a flat-cut foam section, there is significant friction with the air when rotating at high speeds, resulting in substantial noise generation when the fan operates at elevated velocity ranges (Fig. 21 and Fig. 22).

Regions with turbulence kinetic energy (TKE) dissipation coefficients ranging from 7 to 13 (indicated in yellow to red) demonstrate considerable eddy energy, concentrated just beneath the blade tip, where the shear layer detaches most vigorously. Consequently, the primary source of aerodynamic noise originates from the blade edge and gradually propagates down to the floor of the room along two columns of airflow.

5.3. Noise Reduction Methods

With the same vortex resolution, the vortex region of the rounded tip blade is smaller than that of the unrounded tip blade. The distribution of the turbulent energy dissipation coefficient (TED) indicates that the TED of the rounded tip blade model is higher, suggesting that the vortices are dissipated more rapidly, and the airflow stabilizes sooner of the airflow. A high TED aids in the rapid dissipation of vortices, potentially reducing noise caused by air turbulence. Conversely, a low TED may allow vortices to persist longer, resulting in low-frequency sounds (humming) or undesirable oscillations. The maximum sound intensity at the rounded tip blade is 53 dB, a reduction of 20 dB compared to the unrounded blade (Fig. 23 and Fig. 24).

At the tip-rounded blade version operating at a speed of 225 rpm, the noise level was reduced by more than 20 dB, specifically from 75 dB in the unrounded tip version to over 53 dB in the rounded tip version. This demonstrates the effectiveness of applying the tip rounding method to dissipate vortices (Fig. 25. and Fig. 26).

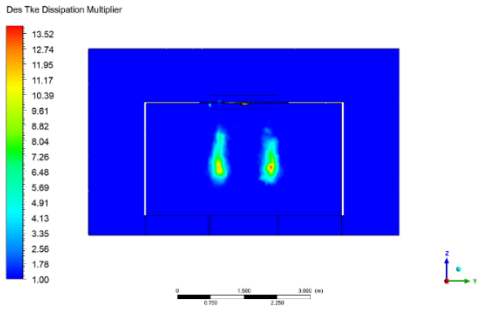

Fig. 21. Des Tke dissipation mulplier

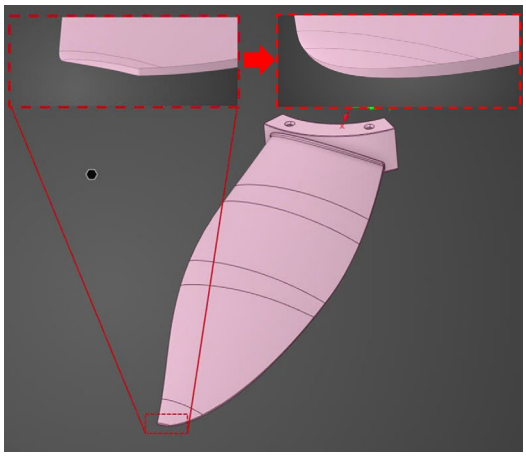

Fig. 23. Noise reduction methods

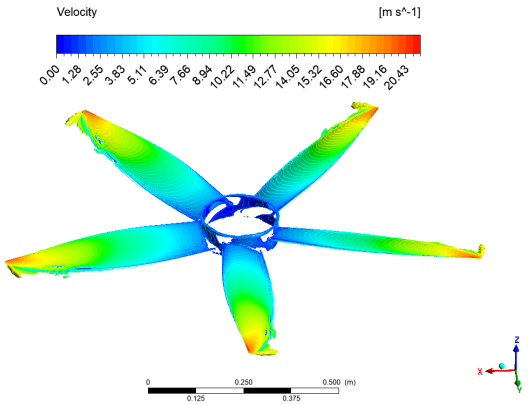

Fig. 22. Velocity field at the surface

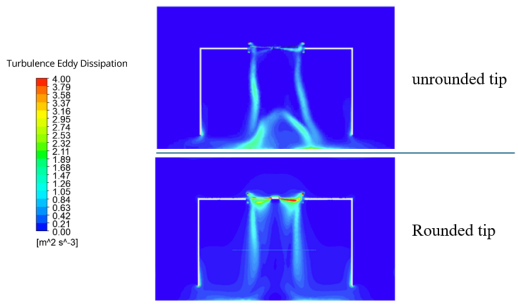

Fig. 24. Turbulence eddy dissipation

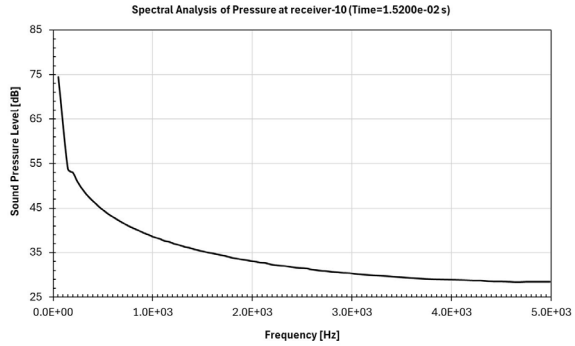

Fig. 25. Unrounded, sound pressure level reaching a threshold of 74.5 dB

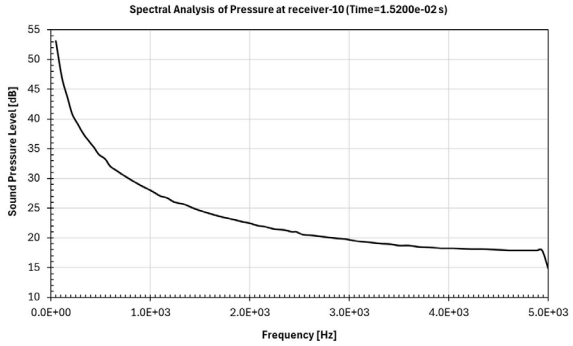

Fig. 26. Rounded tip, sound pressure level reaching a threshold of 53 dB

Fig. 27. Air blade prototype (PC anti-shrink material)

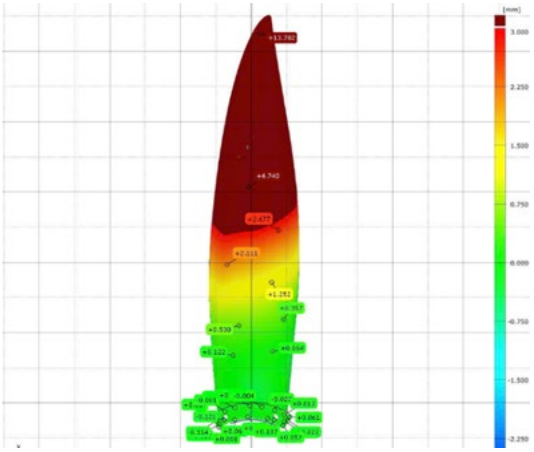

Fig. 28. Results of the comparison between the 3D scan of the physical sample and CAD file

5.4. Experimental Results

The AIR blade model is produced using the plastic injection molding method. The surface of the blade is smooth and visually appealing, and the blade profile adheres to the 3D design specifications. However, due to the heating process inherent in plastic injection molding, the blade experiences shrinkage and warping, with the tip deflection being controlled within a range of less than 20 mm. This result is achieved through the use of 3D scanning of the prototype and comparison with the original design, as illustrated in Fig. 27. The set of three sample blades was measured in a standard measurement chamber, yielding results as shown in Fig. 28, with the outcomes aligning closely with the simulations (error less than 3%).

The test results of the device, conducted in accordance with Vietnamese standards, show that the voltage, frequency, and efficiency meet the required specifications (Table 6).

Table 6. Test results according to Vietnam Standards at Phuc Gia Testing Center

No.	Contents	Results	Evaluation
1	Voltage at EUT when measuring (V)	219.77	Pass
2	Frequency at EUT when measuring (Hz)	50	Pass
3	Fan power consumption (W) - P	22.73	-
4	Air flow of fan (m^3/min) - Q	246.61	-
5	Energy efficiency ratio {m^3/(min/W)} - EER = Q / P	10.85	-
6	Minimum energy efficiency {m^3/(min·W)} - EERmin	3.04	-
7	Energy efficiency index: R = EER / EERmin	3.57	-
8	Energy efficiency grade	5	Pass

6. Conclusion

Regarding the reliability of the computational mesh: the Mesh 4 model with 11.5 million elements demonstrates stable torque convergence (the error between Mesh 3 and Mesh 4.5 is negligible) and a maximum y^+ value of less than 1, fully meeting the requirements of the k–ω SST and DES models. This ensures both accuracy and computational resource efficiency.

Regarding flow and blade load the AIR blade version 2 H14/S12 exhibits the best performance among the variants and aligns with the technological and technical standards for R&D products. The effective operating range at a rotational speed of 220-225 rpm for 5 blades is predicted to be equivalent to 265-270 rpm for 3 blades.

Concerning noise, the AIR blade features an aerodynamic design with a rounded tip that significantly improves the vortex region at the blade edge and the turbulence dissipation coefficient, indicating a more stable airflow and reduced noise levels. It can be stated that this design lives up to its name "Air," as it maintains a noise level below 60 dB, allowing users to experience smooth and comfortable operation.

These analyses not only clarify the aerodynamic principles underlying ceiling fan operation of the ceiling fan but also provide a scientific basis for blade design, rotational speed adjustment, and motor design aligned with the trends of energy-efficient green technology. Future research directions include:

- Applying the LES model to capture smaller-scale vortices in greater detail.

- Investigating the impact of blade shape and distance to the ceiling on acoustic characteristics.

Acknowledgments

This research paper is one of the outcomes of the collaboration between the research team at Hanoi University of Science and Technology and Gcool Joint Stock Company in the field of research and design of high-performance, energy-saving fan models.

References

[1] Ankur. J., Rochan. R. U., Samarth. C., Manish. S, and Sunil. K., Experimental investigation of the flow field of a ceiling fan. ASME 2004 Heat Transfer/Fluid Engineering Summer Conference, Charlotte, North Carolina, USA. (2004).

[2] Parker, D. S., Challahan, M. P. Sonne, J. K., Su, G. H., and Hibbs, B. D., Development of a high efficiency ceiling fan. Florida Solar Center, 1679 Clearlake Road, Cocoa Florida 32922, USA. (2000).

[3] Falahat, A., Numerical and experimental optimization of flow coefficient in tubeaxial fan. International Journal of Multidisciplinary Sciences and Engineering 2(5), pp. 24-29. (2011).

[4] Son. H. Ho, Rosario, L., and Rehman, M., Thermal comfort enhanchment by using a ceiling fan. Applied Thermal Engineering 29(9), 1648-1656. (2009) https://doi.org/10.1016/j.applthermaleng.2008.07.015

[5] Kusano, K., Jeong, J., Furukawa, M., 1012 detached eddy simulation and prediction of aerodynamic sound in a half-ducted propeller fan. The Proceedings of the Fluids Engineering Conference, 2010(0),283–284. (2010). https://doi.org/10.1299/jsmefed.2010.283

[6] Kusano, Kazuya, Yamaguchi Hiroki, Hatakenaka Kisho, Sakoda Kenichi, Yanagi Ryushin, Furukawa Masato, Adjoint-based aeroacoustic shape optimization using lattice Boltzmann method for suppressing cavity tones at low Mach numbers. Journal of Sound and Vibration. 611. 119131. (2025).

[7] Vaezi, Erfan, S. Amirreza S. Madani, and Amir Keshmiri, Effects of winglet cant angle on wing aerodynamics and aeroacoustics: A parametric study. (2024).

[8] Xu Hang, Weiqi Wang, Chen Xi, Zhao, Qijun., Numerical analysis of aeroacoustic characteristics for coaxial counter rotating propellers considering the self-interference effect. Aerospace Science and Technology.(2024). 152. 109358.

[9] Haolin Zhi, Deng Shuanghou, Xiao Tianhang, QIN Ning, GUO Jingliang, Trade-off between propeller aerodynamics and aeroacoustics using unsteady adjoint-based design optimization. Chinese Journal of Aeronautics. 103481. (2025).

[10] Greschner Björn, Thiele Frank, Jacob Marc, Casalino, Damiano, Prediction of sound generated by a rod-airfoil configuration using a cubic EASM-DES and the generalised Lighthill/FW-H Analogy, Computer and Fluids. 37. 402-413 (2008).

[11] Hirschberg, A., and Rienstra, S. W., An introduction to aeroacoustics, Eindhoven University of Technology, Eindhoven, The Netherlands (2004).

[12] Maizi, M., Mohamed, M. H., Dizene, R., and Mihoubi, M. C., Noise reduction of a horizontal wind turbine using different blade shapes, Renewable Energy, 117, pp. 242-256 (2018).

[13] Mockett, C., A comprehensive study of detached-eddy simulation, Ph.D. Thesis, Technische Universität Berlin, Berlin, Germany (2009).

[14] Michel, U., Eschricht, D., Greschner, B., Knacke, T., Mockett, C., and Thiele, F., Advanced DES Methods and Their Application to Aeroacoustics, in Notes on Numerical Fluid Mechanics and Multidisciplinary Design, vol. 108, Springer, Berlin, Heidelberg (2010).

[15] Bleier, F. P., Fan Handbook: Selection, Application, and Design, 1st ed., McGraw-Hill Education, New York, NY, USA (1998).